J. Fluid Mech. (1974), *vol.* 65, *part* 3, *pp.* 561–579
Printed in Great Britain

Universal similarity at high grid Reynolds numbers

By J. SCHEDVIN,

Department of Applied Mechanics and Engineering Sciences,
University of California, La Jolla

G. R. STEGEN

Department of Geological and Geophysical Sciences, Princeton University,
Princeton, New Jersey 08540

AND C. H. GIBSON

Department of Applied Mechanics and Engineering Sciences,
University of California, La Jolla

(Received 16 November 1973)

Kolmogorov's second hypothesis has been examined for the case of turbulence generated behind a very large grid. The turbulent Reynolds number $R_\lambda = 280$ was sufficient to obtain a short inertial subrange. The one-dimensional subrange constant $\alpha_1 = 0{\cdot}48 \pm 0{\cdot}06$ is in agreement with recent determinations made in geophysical flows. Isotropy was tested by comparing the transverse velocity spectrum with the transverse spectrum predicted from the longitudinal spectrum using the isotropic relations. The comparison showed the flow to be isotropic everywhere except at the largest scales.

It was observed that at high wavenumbers the spectra were attenuated by effects of finite wire length. The wire-length corrections suggested by Wyngaard (1968) were found to be inadequate. New corrections based on experimentally determined universal spectra are proposed.

1. Introduction

Over the past 20 years a significant fraction of turbulence research has been devoted to the study and application of Kolmogorov's universal similarity hypotheses, which assimilate a great variety of turbulent flows into a single unified theoretical structure. Kolmogorov's second hypothesis predicts a specific form for the universal velocity spectrum called the 'inertial subrange', valid for wavenumbers k between the large-scale (k_0) energy-containing wavenumber region and the small-scale (k_D) viscous dissipation region. If such a wavenumber regime exists, its spectrum will depend only on k and the flux of energy from the larger to smaller scales at the average dissipation rate ϵ. The 'inertial subrange' for the one-dimensional energy spectrum follows by dimensional analysis:

$$\Phi_1(k_1) = \alpha_1 \epsilon^{\frac{2}{3}} k_1^{-\frac{5}{3}} \quad \text{for} \quad k_0 \ll k_1 \ll k_D, \tag{1}$$

where

$$\overline{u_1^2} = \int_0^\infty \Phi_1(k_1)\, dk_1. \tag{2}$$

When the spectrum is normalized with the Kolmogorov length scale $\eta = (\nu^3/\epsilon)^{\frac{1}{4}}$ and time scale $t = (\nu/\epsilon)^{\frac{1}{2}}$,

$$\Phi_1(k_1\eta) = \alpha_1(k_1\eta)^{-\frac{5}{3}}. \tag{3}$$

Equation (3) is a special case of the universal form which follows from Kolmogorov's first universal similarity hypothesis. Kolmogorov (1962) has refined his earlier hypotheses to include the influence of the spatial variability of ϵ (see Gibson, Stegen & Williams 1970; Gibson, Stegen & McConnell 1970). However, the effect appears to be negligibly small, so many authors (for example, Pond *et al.* 1971) continue to use (1) for the analysis and interpretation of experimental measurements. Consequently, it is important to know the value of the universal constant α_1 which characterizes the inertial subrange of the velocity spectrum.

To obtain a reliable value for the Kolmogorov inertial subrange constant α_1 both the velocity spectra and the average dissipation rate ϵ must be accurately determined. Traditionally, the greatest uncertainty in determining α_1 has been due to the difficulty of measuring ϵ. In this study, several techniques have been used to determine ϵ, including the decay of turbulent energy, correlation with other grid-generated turbulent flows (Friehe & Schwarz 1970), and integration of velocity-derivative spectra which have been corrected for effects of finite wire length.

Implicit in (1) is the assumption that the turbulent Reynolds number is large enough for the energy scale $L_0 = 1/k_0$ to be much larger than η. The turbulent Reynolds number R_λ is defined by

$$R_\lambda = (\overline{u^2})^{\frac{1}{2}}\lambda/\nu, \tag{4}$$

where the Taylor microscale λ is given by

$$\lambda = [15\nu\overline{u^2}/\epsilon]^{\frac{1}{2}}. \tag{5}$$

Corrsin (1958) and Bradshaw (1967) suggested that a value for R_λ of 200–300 is required for the existence of an inertial subrange. R_λ for grid-generated turbulence is usually less than 130, while for laboratory jets or wakes R_λ may be as large as 1000. In contrast, geophysical flows (atmospheric boundary layers, tidal channels, etc.) have values of R_λ at least an order of magnitude larger. For this reason, values of α_1 in the range 0·4–0·5 estimated from oceanic and atmospheric measurements were widely accepted (Pond *et al.* 1966).

Recent measurements by Gibson, Stegen & Williams (1970) yielded values of α_1 in the range 0·6–0·7 under conditions similar to those of Pond *et al.* (1966). The only laboratory study of high Reynolds number turbulence available for comparison was that of Kistler & Vrebalovich (1966), which gave even larger values of $\alpha_1 = 0{\cdot}7$–$0{\cdot}9$. Consequently, it seemed appropriate to try and resolve the apparent discrepancy between these results by repeating the Kistler & Vrebalovich experiment on high Reynolds number grid turbulence. This was carried out by one of us (GRS) using the large wind tunnel at Colorado State University. The grid Reynolds numbers R_M ($\equiv UM/\nu$, where M is the mesh size) were in the range $2{\cdot}0$–$4{\cdot}0 \times 10^5$, which overlaps the lower range of Reynolds numbers used by Kistler & Vrebalovich.

In addition to the determination of α_1, an important result of the study was the development of an empirical correction for effects of finite hot-wire length. During the course of the analysis it was concluded that correction for effects of finite wire length was crucial to the proper evaluation of the data. Currently available estimates for wire-length corrections (Wyngaard 1968) were found to be inadequate. These estimates were based on theoretical rather than experimentally determined high wavenumber spectra shapes, and are quite sensitive to the analytical representation of the spectra at high wavenumbers.

2. Experimental arrangement

The measurements were made at Colorado State University in a closed-circuit wind tunnel with a very large test section ($1{\cdot}8 \times 1{\cdot}8 \times 24{\cdot}3$ m). Designed as a low turbulence wind tunnel, this facility is normally used for studies of the atmospheric boundary layer and mesoscale meteorological simulations (Cermak 1971).

To adapt this wind tunnel for the study of grid-generated turbulence a number of physical changes were carried out. The artificial surface roughness at the entrance of the wind tunnel was removed and the entrance faired to provide a slow smooth contraction. The instrument carriage normally used was moved to the farthest possible downstream position, where it would not influence the measurements. The carriage tracks which run along the inside of the tunnel were covered with temporary vertical walls.

A biplane grid with a square mesh ($M = 22{\cdot}9$ cm) and square (3·81 cm) rods was installed one tunnel diameter downstream from the tunnel entrance. The grid solidity was 0·30, slightly less than the value of 0·34 typical of earlier grid experiments. With the grid installed, the wind tunnel had a maximum speed of 32 m/s. The heating of the flow by the blower mechanism made it necessary to provide continuous cooling of the air stream. With cooling, a nominal steady air temperature of 1 °C could be maintained. This low temperature produced a slight decrease in kinematic viscosity resulting in a modest increase in grid Reynolds number. When the tunnel was operating at maximum speed and cooling, a grid Reynolds number R_M greater than 400000 could be obtained. The mean velocity U and velocity fluctuations u and v in the longitudinal and transverse directions were measured at downstream locations $X/M = 35$, 38, 40 and 41, where X is the distance from the grid. The measurements were made at nominal speeds of 13·2, 24·0 and 28·8 m/s and grid Reynolds numbers of $1{\cdot}89 \times 10^5$, $3{\cdot}35 \times 10^5$ and $4{\cdot}02 \times 10^5$.

A Pitot tube and a hot-wire sensor were positioned in the centre of the tunnel on a vertical stand bolted to the wind-tunnel floor. This arrangement was chosen to minimize wind-tunnel blockage. However, to make measurements at different values of X/M, it was necessary to shut down the wind tunnel before moving the probe stand. Special care was taken to ensure that the test conditions could be repeated after moving the probes to a new location. A second Pitot probe was fixed at the far downstream end of the tunnel. Using this probe as a reference, it was possible to repeat the speeds at different X/M's to within ± 22 cm/s. The air stream temperatures were repeatable to within ± 1 °C. During a given run,

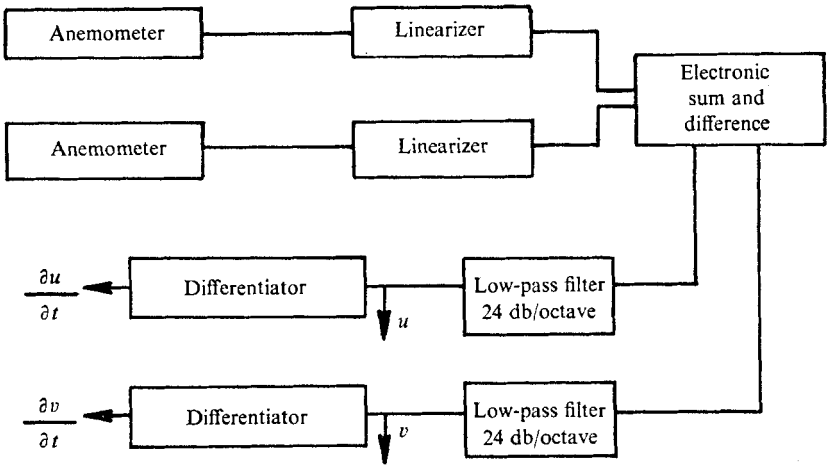

FIGURE 1. Block diagram of velocity measuring and signal conditioning system.

the air stream temperature was held constant to within $\pm 0{\cdot}5\,^{\circ}\mathrm{C}$. All measurements were made at night to minimize the influence of atmospheric variables on the tunnel operation.

The u and v velocity fluctuations were measured with a standard X-wire array (Thermo-Systems, Inc., Model 1241-T1.5). The sensors were operated in the constant-resistance mode using a DISA Model 55D01 constant-temperature anemometer system. Owing to the large size of the tunnel, 25 m probe cables were required between the anemometer system and the sensors. This required the use of additional impedance in the anemometer bridge to ensure stable operation of the anemometer. Anemometer output signals were linearized and their sensitivities matched with DISA Model 55D10 linearizers. The velocity measuring system had a frequency response of -3 db at 30 kHz.

Voltage signals proportional to u and v were obtained directly using an electronic sum-and-difference circuit. The X-wire and associated electronics were calibrated in a laminar jet calibrator. For probe yaw angles up to $\pm 10^{\circ}$ the output followed a simple cosine response with equal sensitivities for u and v. At each X/M the anemometer system was calibrated *in situ* using the adjacent mounted Pitot probe.

Time derivatives $\partial u/\partial t$ and $\partial v/\partial t$ of the velocity fluctuations were generated from the u and v signals with electronic differentiators. Voltage signals corresponding to the velocity fluctuations and their derivatives were recorded on an AMPEX FR1300, FM tape recorder. The complete velocity measuring system and signal conditioning equipment are shown in figure 1.

3. Data analysis

The primary intent of this paper is to examine universal similarity in grid-generated turbulence at high Reynolds numbers. The analysis presented here is concerned with measurements taken at the highest mean speed obtained at the farthest downstream location ($U = 28{\cdot}9$ m/s, $X/M = 41$). The grid Reynolds

$U = 28{\cdot}9$ m/s	$\nu = 1{\cdot}62 \times 10^{-5}$ m^2/s
$X/M = 41$	$R_M = 4{\cdot}08 \times 10^5$
$u' = 0{\cdot}650$ m/s	$v' = 0{\cdot}632$ m/s
$(\partial u/\partial x)' = 74{\cdot}9$ s^{-1}	$(\partial v/\partial x)' = 97{\cdot}4$ s^{-1}

TABLE 1. Summary of test conditions. A prime denotes a root-mean-square value.

number for these measurements was $R_M = 408\,000$. A summary of r.m.s. values of the measured quantities is given in table 1. The time derivatives $\partial u/\partial t$ and $\partial v/\partial t$ were converted to space derivatives using the instantaneous space–time transformation $\partial/\partial t = +U\,\partial/\partial x$. This assumption is justified for steady low intensity turbulent flows such as grid-generated turbulence (Lumley 1965). Although the ratio $u'/v' = 1{\cdot}03$ is close to the isotropic value of 1·00, it should be noted that the ratio $\{(\partial u/\partial t)'/(\partial v/\partial t)'\}^2 = 0{\cdot}59$ is significantly larger than the value of 0·50 expected for locally isotropic turbulence. It will be shown below that this apparent departure from local isotropy is attributable to effects of finite wire length.

3.1. *Dissipation calculation*

The average value of the local dissipation is given by

$$\epsilon = 2\nu\,\overline{e_{ij}e_{ij}}, \tag{6}$$

where

$$e_{ij} = \tfrac{1}{2}(\partial u_i/\partial x_j + \partial u_j/\partial x_i), \tag{7}$$

in which summation of repeated indices is stipulated.

Far downstream of the grid, the turbulence is relatively homogeneous in the transverse directions and approximately isotropic. Assuming isotropy, (6) can be written in several forms, including

$$\epsilon = 15\nu\overline{(\partial u/\partial x_1)^2} \tag{8}$$

and

$$\epsilon = \nu\{3\overline{(\partial u/\partial x_1)^2} + 6\overline{(\partial v/\partial x_1)^2}\}. \tag{9}$$

The first expression only requires the measurement of the longitudinal velocity fluctuations. The second expression includes the measurement of the transverse velocity fluctuations, and may be used to compensate for slight anisotropy of the turbulence field. Both expressions for ϵ will be used in this study.

3.1.1. *Decay of turbulent energy.* The dissipation rate ϵ can be determined directly from a measurement of the decay of turbulent energy. The rate of turbulent energy decay in an unsheared homogeneous turbulent flow is given by

$$\tfrac{1}{2}\,d\overline{q^2}/dt = -\epsilon, \tag{10}$$

in which $\overline{q^2} = \overline{u^2} + \overline{v^2} + \overline{w^2}$, u, v and w being the fluctuating components of the longitudinal and transverse velocities. Assuming transverse isotropy in a grid flow, and using Taylor's hypothesis, we can express the dissipation rate as

$$\epsilon = -\tfrac{1}{2}U d(\overline{u^2} + \overline{2v^2})/dx_1. \tag{11}$$

The values of $\overline{u^2}$ and $\overline{v^2}$ were within 4 % of each other under all test conditions. We have, therefore, chosen to fit a decay law to $\overline{q^2}$ rather than individually to $\overline{u^2}$

n \ X_0/M	0	2	4
−1·00	1·92	2·01	2·11
−1·25	2·35	2·46	2·58

TABLE 2. Variation of estimate of dissipation ϵ (m^2/s^3) from (13) with several choices of X_0/M and n.

and $\overline{v^2}$ as has been done by previous investigators. A least-squares fit of the data was made to the expression

$$\overline{q^2} = +A(X/M - X_0/M)^n, \tag{12}$$

where X_0/M is the virtual origin at which the turbulence intensity is infinite.

Using (11) and (12), the dissipation rate can be expressed as

$$\epsilon = -\frac{nAU}{2M}(X/M - X_0/M)^{n-1}. \tag{13}$$

The best value of the exponent to use in the decay equation is somewhat uncertain. In early studies $n = -1$ was used; however, Comte-Bellot & Corrsin (1966) have suggested $n \approx -1{\cdot}25$. All the data were fitted to (12) using values of n between 0·90 and 1·40 and values of X_0/M between 0 and 10·0. The best fit was obtained with $n = -1{\cdot}0$, $X_0/M = 0$ and with $A = 5{\cdot}12 \times 10^5\ \mathrm{cm^2/s^3}$. These values yield $\epsilon = 1{\cdot}92 \times 10^4\ \mathrm{cm^2/s^3}$ at $X/M = 41$. However, because of the small range of X/M and corresponding small changes in q^2, a range of parameters gave equally satisfactory fits to the data. Table 2 gives the estimates of ϵ for $n = -1{\cdot}0$ and $-1{\cdot}25$ and $X_0/M = 0$, 2 and 4, all of which gave good fits to the data. All the estimates are in the range $\epsilon = 2{\cdot}2 \pm 0{\cdot}3 \times 10^4\ \mathrm{cm^2/s^3}$.

A least-squares fit was also made to measured dissipation rates calculated from (9), using an equation of the same form as (13):

$$\epsilon = B(X/M - X_0/M)^{n-1}. \tag{14}$$

The best fit was again obtained with $n = -1$ and $X_0/M = 0$, and with $B = 2{\cdot}19 \times 10^7\ \mathrm{cm^2/s^3}$. The value of ϵ at $X/M = 41$ from (14) is $1{\cdot}30 \times 10^4\ \mathrm{cm^2/s^3}$. This value of ϵ is 40 % less than the value predicted using the energy-decay technique. This low value prompted the subsequent investigation of wire-length corrections (§ 3.1.3).

3.1.2. *Correlation of grid-generated turbulence experiments.* Friehe & Schwarz (1970) have suggested a method for correlating the results of different experiments on grid-generated turbulence. They demonstrated that the dimensionless variable

$$\epsilon' = \epsilon M/(\overline{u^2} + \overline{2v^2})\,U \tag{15}$$

could be used to correlate measurements made using both round and square rod grids. For $X/M = 41$ the value of ϵ' obtained from Friehe & Schwarz's plot yields a dissipation rate for the present experiment of $\epsilon = 2{\cdot}4 \pm 0{\cdot}3 \times 10^4\ \mathrm{cm^2/s^3}$, in reasonable agremeent with the value obtained from the decay law.

3.1.3. *Wire-length corrections.* In § 3.1.1 we found that the dissipation rate estimated from the velocity derivatives was significantly lower than the estimate obtained using the velocity fluctuations. Since the integral of the derivative spectrum is very sensitive to the spectral shape at high wavenumbers, attenuation of the spectrum by effects of finite wire length was suspected. Wyngaard (1968) has proposed a theoretical expression for correcting velocity spectra for the averaging due to finite wire length l_w. Using the universal spectrum function proposed by Pao (1965) he derived an expression relating the ratio of the true to the measured one-dimensional velocity spectra obtained with a X-wire. This relation depends on the ratios η/l_w and d/l_w, where d is the perpendicular separation of the wires and η is the Kolmogorov length scale. Using the value of the dissipation estimated from the decay law, the length scale for the present data is $\eta = 0{\cdot}020$ cm, which gives $\eta/l_w = 0{\cdot}16$. The corrections for our particular case $\eta/l_w = 0{\cdot}16$ and $d/l_w = 0{\cdot}4$ were not computed by Wyngaard. In order to make a comparison we choose available corrections for $\eta/l_w = 0{\cdot}1$ and $d/l_w = 0{\cdot}5$ for the longitudinal spectrum and $\eta/l_w = 0$ and $d/l_w = 0{\cdot}5$ for the transverse spectrum. The corrections corresponding to these values should be slightly larger than those needed for our data as they represent longer wires with greater wire separation.

The wire-length corrections were applied to the velocity and velocity-derivative spectra, which can be integrated to give the mean-square velocity and velocity derivatives as follows:

$$\overline{u^2} = \int_0^\infty \Phi_1(k_1)\,dk_1, \quad \overline{v^2} = \int_0^\infty \Phi_2(k_1)\,dk_1, \tag{16), (17}$$

$$\overline{\left(\frac{\partial u}{\partial x_1}\right)^2} = \int_0^\infty \Psi_1(k_1)\,dk_1, \quad \overline{\left(\frac{\partial v}{\partial x_1}\right)^2} = \int_0^\infty \Psi_2(k_1)\,dk_1. \tag{18), (19}$$

The average dissipation is calculated from the integrals of the velocity-derivative spectra through substitution into (8) and (9):

$$\epsilon = 15\nu \int_0^\infty \Psi_1(k_1)\,dk_1 \tag{20}$$

or

$$\epsilon = 3\nu \int_0^\infty \Psi_1(k_1)\,dk_1 + 6\nu \int_0^\infty \Psi_2(k_1)\,dk_1. \tag{21}$$

Evaluation of (20) using the measured spectrum gives $\epsilon = 1{\cdot}36 \times 10^4\,\mathrm{cm^2/s^3}$ while (21) yields $\epsilon = 1{\cdot}20 \times 10^4\,\mathrm{cm^2/s^3}$. After applying Wyngaard's spectral correction to $\Psi_1(k_1)$ and $\Psi_2(k_1)$ the corrected dissipation values obtained were $\epsilon = 1{\cdot}64 \times 10^4\,\mathrm{cm^2/s^3}$ from (20) and $\epsilon = 1{\cdot}4 \times 10^4\,\mathrm{cm^2/s^3}$ from (21). These values are still considerably smaller than those obtained from the decay law and the Friehe & Schwarz correlation. This difference prompted us to try a different wire-length correction procedure. This correction was made by comparing our normalized but uncorrected spectra with other normalized spectra of universal form. The Kolmogorov scales used to normalize our measured spectra were computed using the dissipation rate obtained from integrating the respective derivative spectra as in (20) and (21).

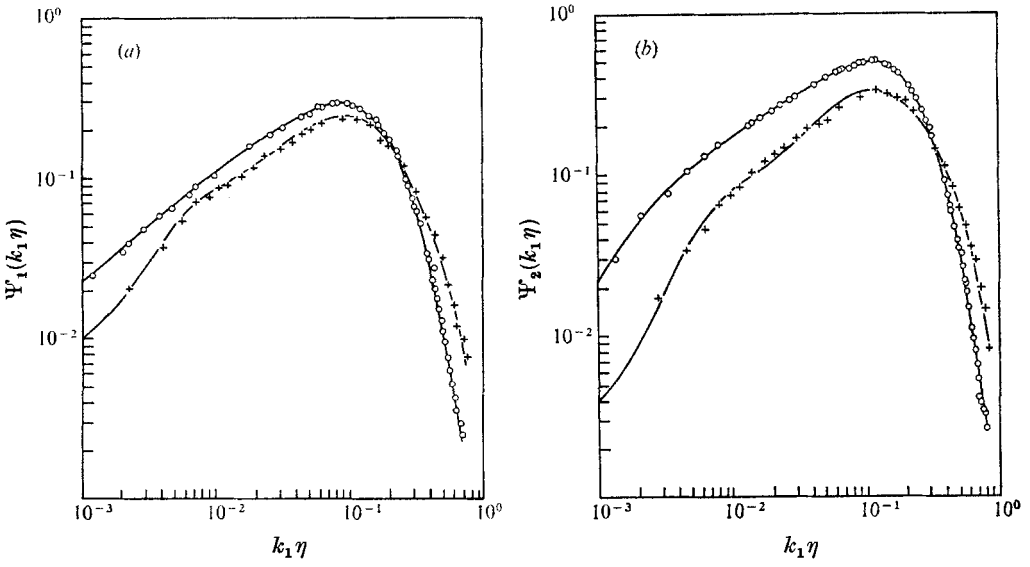

FIGURE 2. Normalized (*a*) *du/dt* and (*b*) *dv/dt* spectra and reference wake spectra. ○, grid data points; +, reference cylinder wake data points (Champagne & Wygnanski); ——, polynomial fits.

The reference spectra used for this comparison were from unpublished measurements made by F. H. Champagne & I. J. Wygnanski in a cylinder wake at a downstream distance of 299 cylinder diameters. These spectra were felt to require only small wire-length corrections since the wires were very short with respect to η, having a ratio $\eta/l_w = 0{\cdot}75$.

The u wake spectrum was used to correct our longitudinal spectrum and the w_τ wake spectrum (w_τ being in the direction parallel to the cylinder axis) to correct our transverse spectrum. The reference and measured spectra normalized with their respective Kolmogorov length and time scales are compared in figures 2(*a*) and (*b*).

Champagne (1973) has compared the reference spectra with the spectra from a variety of low intensity turbulent flows. Good agreement as to shape and magnitude of the second and fourth moments of the velocity spectra suggests that the reference spectra used were indeed reasonably universal in form. The reference wake spectra were obtained at a turbulence Reynolds number $R_\lambda = 258$, which is near the value for the present data of $R_\lambda = 280$ (based on the dissipation rate calculated from the decay law).

Empirical wire-length corrections were made for both the *du/dx* and *dv/dx* spectra. For this purpose least-squares polynomial fits were computed for the normalized cylinder wake reference spectra. Polynomial fits were also made to our uncorrected unnormalized derivative spectra Ψ'_1 and Ψ'_2, which were then normalized and compared with the second moments of the reference spectra. Through an iterative comparison procedure, wire-length corrections were made to the Ψ'_1 and Ψ'_2 spectra, in the region of normalized wavenumbers from about 0·05 to 0·7.

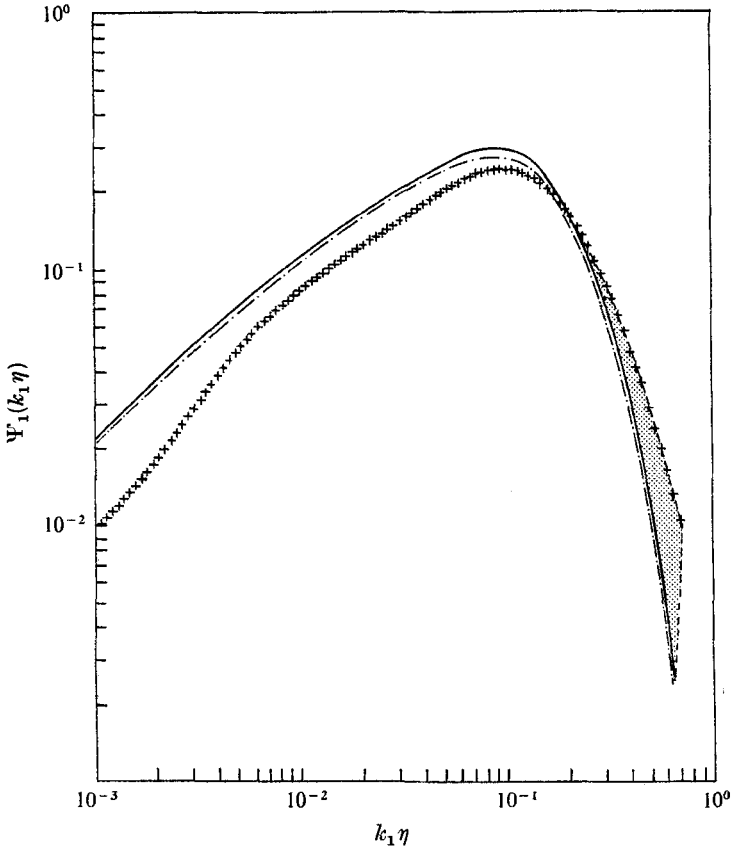

FIGURE 3. Empirical wire-length correction for u spectrum using iteration method. +, points on polynomial fit to reference spectrum; ——, polynomial fit to uncorrected grid data; – – –, grid data corrected to reference spectrum; —·—, grid data renormalized with new dissipation value; ▒▒, increase in area under derivative spectrum.

It was felt that the universality of spectral shape between the present data and the reference spectra should be most valid at wavenumbers above the low end of the inertial subrange. The present data indicate that the inertial subrange extends to a normalized wavenumber of at least 0·05, which was taken as the lower limit for our correction. Also, Wyngaard's correction used above indicated the spectral error for the measured spectra to be less than 2 % below a normalized wavenumber of 0·07. Therefore, the corrections will not be sensitive to the specific value of the cut-off wavenumber chosen for the iteration procedure. The upper limit for corrections was taken to be a normalized wavenumber of 0·7, corresponding to the 15 kHz low-pass filter used when the data were recorded.

The iteration procedure used to obtain an empirical correction is shown in figure 3 for the Ψ_1 spectrum. The polynomial fits made to the measured spectra were normalized using the uncorrected dissipation obtained from the integral of the respective derivative spectrum. Beginning at the large wavenumber limit of 0·7 the derivative spectral points were corrected upwards to the value of the reference spectrum at the same wavenumber. This was continued towards smaller

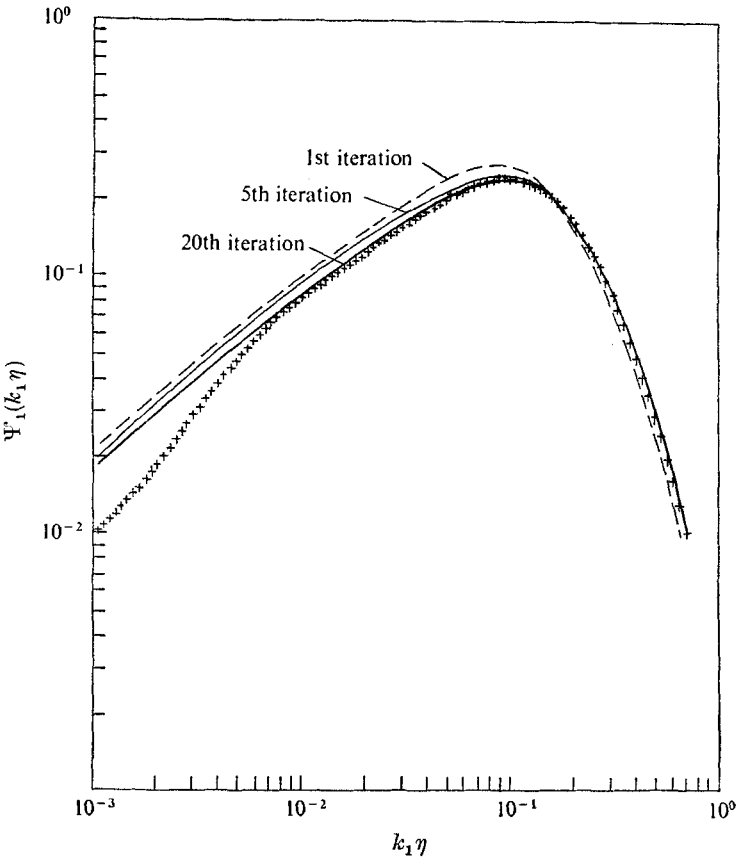

FIGURE 4. Convergence of empirical wire-length correction iteration procedure. +, reference spectrum; – – –, first iteration; ——, fifth or twentieth iteration.

wavenumbers until the cross-over point of the derivative and reference spectra was reached, at which point the correction factor is 1·0. From the cross-over point towards high wavenumbers, the corrected measured spectrum was thus taken equal to the reference spectrum, and below the cross-over point the measured spectrum remained unchanged. These corrections were made solely for the purpose of recalculating ϵ.

This procedure increased the area under the derivative spectrum as shown by the shaded area in figure 3. From this increase in area a new, larger dissipation was calculated such that when the corrected derivative spectrum was re-normalized its area would again be equal to that under the reference spectrum. The corrected dissipation ϵ_C is obtained from the ϵ used for the previous normalization using

$$\epsilon_C = \epsilon \int_0^\infty \Psi_{1C}(k_1\eta)\, d(k_1\eta) \Big/ \int_0^\infty \Psi_{1R}(k_1\eta_R)\, d(k_1\eta_R), \tag{22}$$

where Ψ_{1C} is the Ψ_1 spectrum corrected to the reference spectrum Ψ_{1R}. The integrations were performed over the normalized wavenumber region from 0·001 to 0·7.

When a corrected dissipation value ϵ_C had been obtained, it was used to renormalize the uncorrected derivative spectrum Ψ_1. The correction to the reference spectrum was then repeated. The larger, corrected dissipation ϵ_C causes the Ψ_1 spectrum to be shifted down slightly and towards smaller wavenumbers from its previous position. The process of renormalization, spectral correction and calculation of a new dissipation was continued until the area under the corrected spectrum converged to within 2% of the area under the reference spectrum. Convergence of the corrected Ψ_1 spectrum towards the reference spectrum is shown in figure 4 for the first, fifth and twentieth iterations. The results of the final iteration give the corrected dissipation and spectrum. It can be seen that by the last iteration the agreement between the shapes of the reference and measured spectra is fairly good in the region of normalized wavenumbers $0{\cdot}006 < k_1\eta < 0{\cdot}05$, where no spectral corrections were made. The ratio of the corrected to uncorrected spectral values gives the empirical wire-length correction *vs.* wavenumber. The present empirical wire-length corrections are compared with the previously used Wyngaard corrections in figures 5(*a*) and (*b*). The empirical corrections are significantly larger at high wavenumber than Wyngaard's. The sudden approach to 1·0 of the empirical corrections at small wavenumbers is an artifact of the small wavenumber limit of the empirical correction procedure.

Dissipation values were calculated from the empirically corrected Ψ_1 and Ψ_2 spectra. Use of Ψ_1 in (20) yielded $\epsilon = 2{\cdot}0 \times 10^4\,\mathrm{cm}^2/\mathrm{s}^3$ while use of Ψ_1 and Ψ_2 in (21) gave $\epsilon = 2{\cdot}4 \times 10^4\,\mathrm{cm}^2/\mathrm{s}^3$. These corrected values of the dissipation rate agree well with the earlier estimates obtained from the decay of turbulent energy and the correlation with other grid-generated flows. This lends further support to the estimates of the dissipation values and also to the empirical wire-length correction. The value of $\epsilon = 2{\cdot}2 \pm 0{\cdot}3 \times 10^4\,\mathrm{cm}^2/\mathrm{s}^3$ obtained from the turbulent energy decay has been used in all following spectral normalizations. This value involves the least assumptions and encompasses the values obtained by the other techniques.

3.2. *Inertial subrange constant*

The existence of an inertial subrange has been demonstrated in a variety of laboratory and naturally occurring flows. However, at present there is no general agreement on the value of the inertial subrange constant α. For example, in atmospheric flows the value for the one-dimensional constant α_1 has slowly increased from 0·46 (Pond, Stewart & Burling 1963) to 0·55 (Paquin & Pond 1971) to 0·60 (McBean, Stewart & Miyake 1971). For the present data we have obtained a value of $\alpha_1 = 0{\cdot}48 \pm 0{\cdot}06$ for $R_\lambda \simeq 280$. This was obtained from our longitudinal spectrum corrected according to the empirical wire-length correction and normalized with the decay law dissipation rate.

The customary method of displaying energy spectra to show an inertial subrange is to plot the spectra *vs.* normalized wavenumber in log–log co-ordinates as shown in figure 6. Our longitudinal velocity spectrum might be interpreted as showing a short region perhaps a decade in length which conforms to the $-\frac{5}{3}$ inertial subrange power law. However, such plots are often deceptive as to the actual agreement with the power law and the apparent extent of the inertial

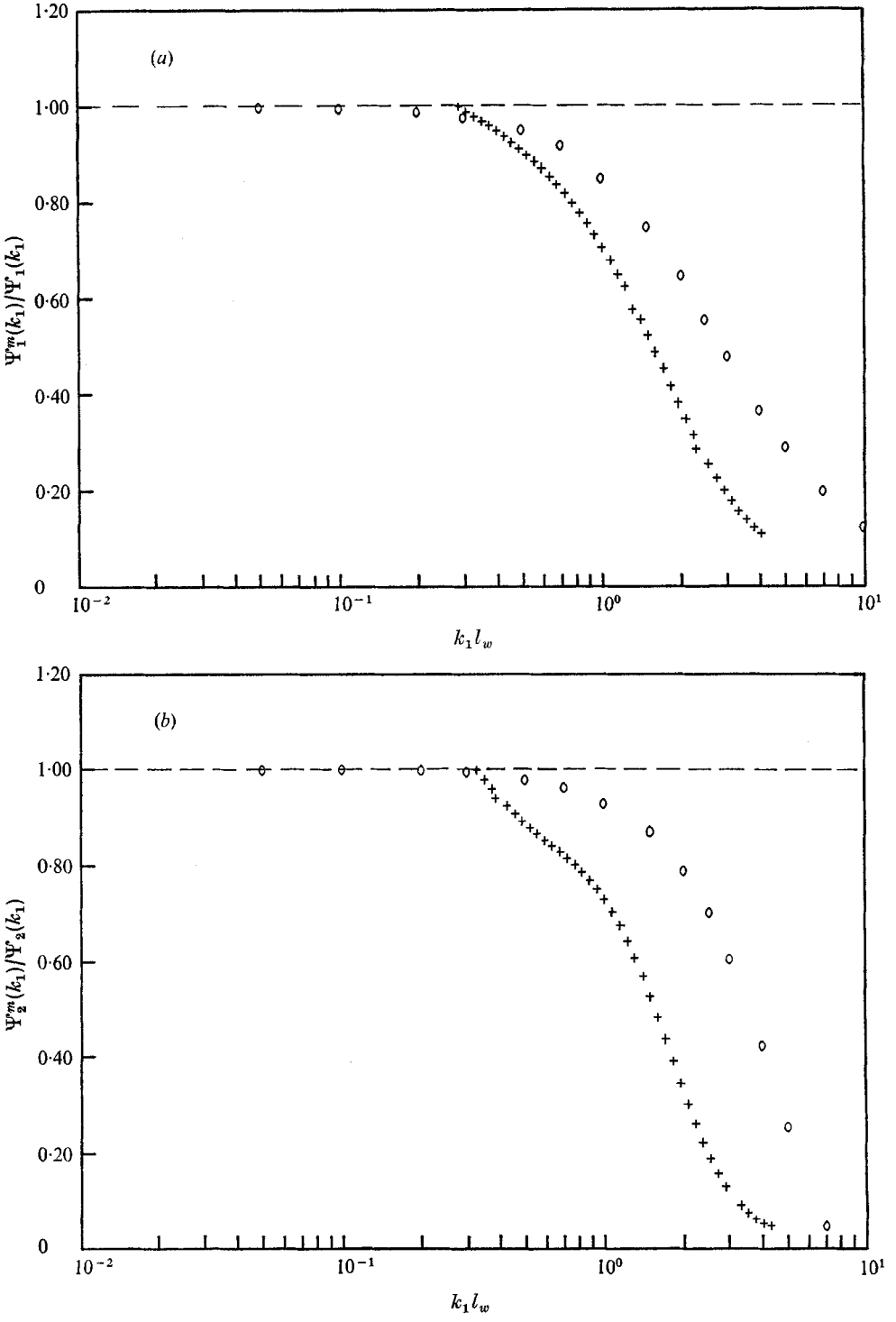

FIGURE 5. Comparison of the empirical and Wyngaard wire-length corrections for (*a*) the longitudinal and (*b*) the transverse spectrum. Ratio of measured to actual spectral values: ◇, Wyngaard's theoretical ratio; +, empirically determined ratio.

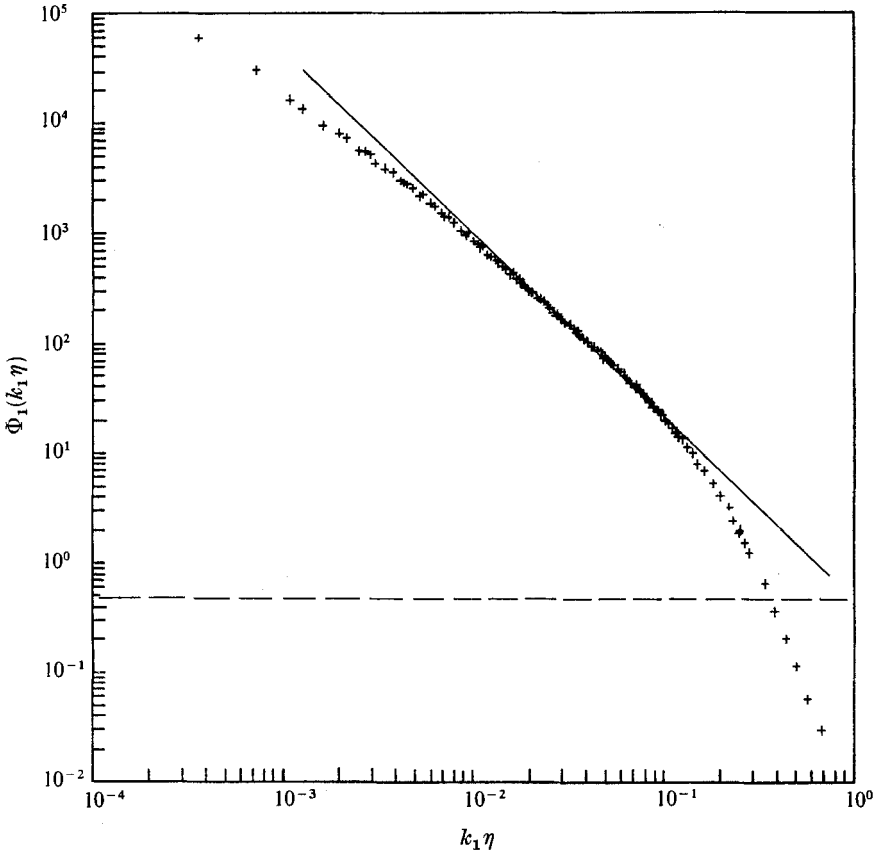

FIGURE 6. Longitudinal spectrum. ——, $-\frac{5}{3}$ inertial subrange spectral slope. Indicated α_1 value is $\approx$ 0·48 from intercept at $k_1\eta = 1$.

subrange. A more stringent test is to plot the spectrum multiplied by the wavenumber raised to the inverse of the expected power law *vs.* the logarithm of the wavenumber. For the case of the inertial subrange we have plotted

$$(k_1\eta)^{\frac{5}{3}} \times \Phi_1(k_1\eta) \text{ } vs. \text{ } \log(k_1\eta)$$

in figure 7. From (3) we see that this corresponds to plotting $\alpha_1(k_1\eta)$ *vs.* $\log(k_1\eta)$. On such a plot, the inertial subrange will appear as a region of constant α_1, the value of α_1 being the value appropriate to the inertial subrange. Figure 7 shows that the inertial subrange which seemed to be indicated in figure 6 is considerably less than a full decade in length, and in fact a true constant region may not exist. Both plots indicate a value of $\alpha_1 \simeq 0{\cdot}48$.

Of the numerous experiments with grid-generated turbulence, only the measurements of Kistler & Vrebalovich (1966) had a large enough Reynolds number (R_λ = 265–670) to allow a determination of α_1. Values of α_1 computed† from their longitudinal spectra lie in the range $0{\cdot}7 < \alpha_1 < 0{\cdot}9$. This range is

† The α_1 values quoted in this paper were calculated from the original data, which were kindly provided by Prof. Kistler.

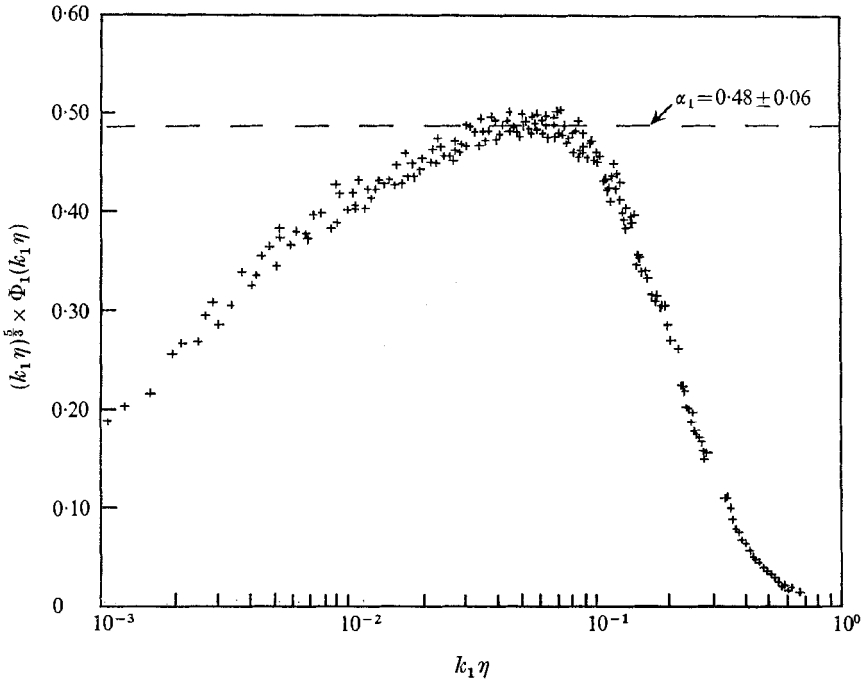

FIGURE 7. Semi-log inertial subrange plot of u spectrum times $(k_1\eta)^{\frac{5}{3}}$. Inertial subrange appears as flat spectral region. $\alpha_1 \approx 0{\cdot}48$.

considerably higher than the present value of 0·48. In fact, at a comparable Reynolds number ($R_\lambda = 265$) their data indicate a value $\alpha_1 \simeq 0{\cdot}9$. This disparity between the present data and those of Kistler & Vrebalovich under similar test conditions contradicts Kolmogorov's prediction of universal similarity in the inertial subrange. The reason for this disagreement is not known. Three of their runs have $\eta/l_w \leqslant 0{\cdot}3$, and therefore require considerable wire-length correction. However, this is not a factor in the normalization of their spectra since they used the measured decay of turbulent energy to determine the dissipation. Therefore, their large α_1 values are most probably due to anomalies in their measured spectra.

In figure 8 the present spectral data are compared in a semi-log inertial subrange plot with two of Kistler & Vrebalovich's spectra and also with low Reynolds number grid data previously reported by Comte-Bellot & Corrsin (1971) and Stewart & Townsend (1951). In the higher wavenumber region the present data show good agreement with the shape of the lower Reynolds number spectra. The spectra of Kistler & Vrebalovich are not in as good agreement at high wavenumbers. This may be due to effects of finite wire length for the $R_\lambda = 670$ ($R_M = 2{\cdot}4 \times 10^6$) data for which $\eta/l_w = 0{\cdot}13$; however, wire length should not have affected their data at $R_\lambda = 265$ ($R_M = 6{\cdot}7 \times 10^5$) for which $\eta/l_w = 0{\cdot}95$.

A gradual increase in normalized spectral values at low wavenumbers with increasing Reynolds number is indicated. This is due to the increasing separation between the energy and dissipation scales of the flow, and an approach towards

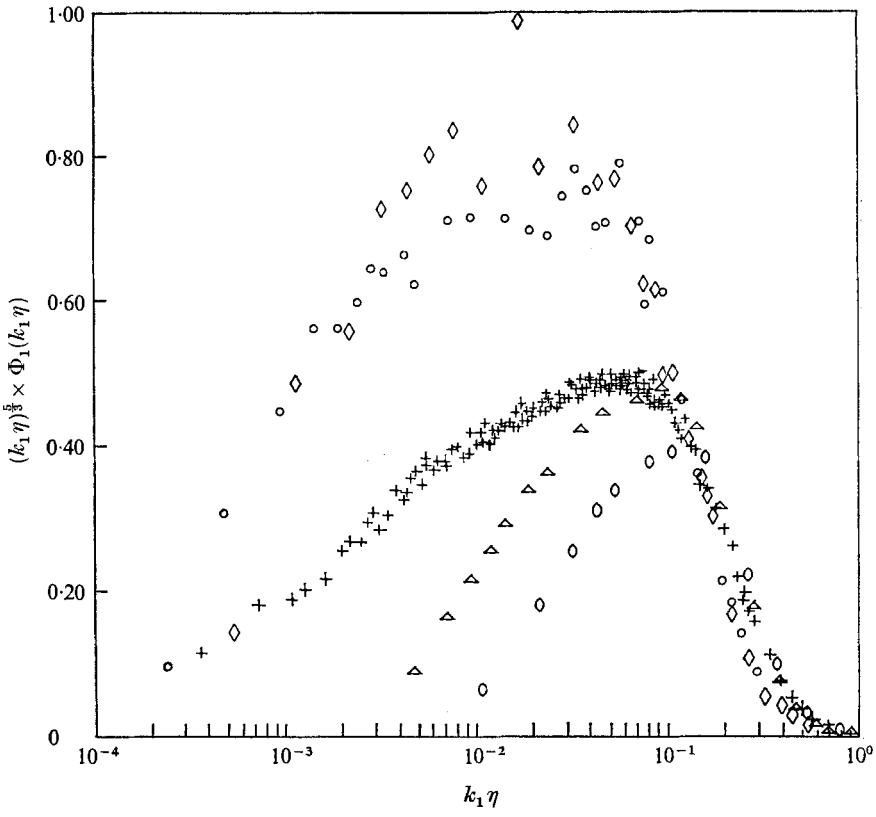

FIGURE 8. Semi-log inertial subrange plot of grid data. +, present data, $R_M = 41{\cdot}0 \times 10^4$; △, Comte-Bellot & Corrsin (1971), $R_M = 3{\cdot}4 \times 10^4$; ◇, Stewart & Townsend, $R_M = 1{\cdot}05 \times 10^4$; ◇, Kistler & Vrebalovich, $R_M = 67{\cdot}0 \times 10^4$; ○, Kistler & Vrebalovich, $R_M = 243{\cdot}0 \times 10^4$.

an inertial subrange between these scales. However, the Kistler & Vrebalovich spectra are inconsistent with this trend, showing a much sharper rise in values. Their two normalized spectra are almost identical in spite of having turbulent Reynolds numbers in the ratio 3 : 1.

3.3. *Isotropy*

The close approximation of grid-generated turbulence to an isotropic field has motivated a number of studies of this flow. The ratio u'/v' of longitudinal to transverse velocity fluctuations is a simple criterion often used to describe the isotropy of grid-generated turbulence. In the present case, $u'/v' = 1{\cdot}03$ compared with 1·07 measured by Comte-Bellot & Corrsin (1966) behind a square-rod grid at $R_M = 1{\cdot}35 \times 10^5$. The lower value in the present case may reflect a small trend towards isotropy with increasing Reynolds number. In any case, the measured ratio is neither a very satisfactory nor illuminating way of describing the actual degee of isotropy exhibited by the flow. The values of u' and v' are integrals of the spectra, and are most sensitive to the large-scale turbulent motions. While it is necessary that $u' = v'$ for the flow to be entirely isotropic, inequality most likely represents anisotropy in the very large scales.

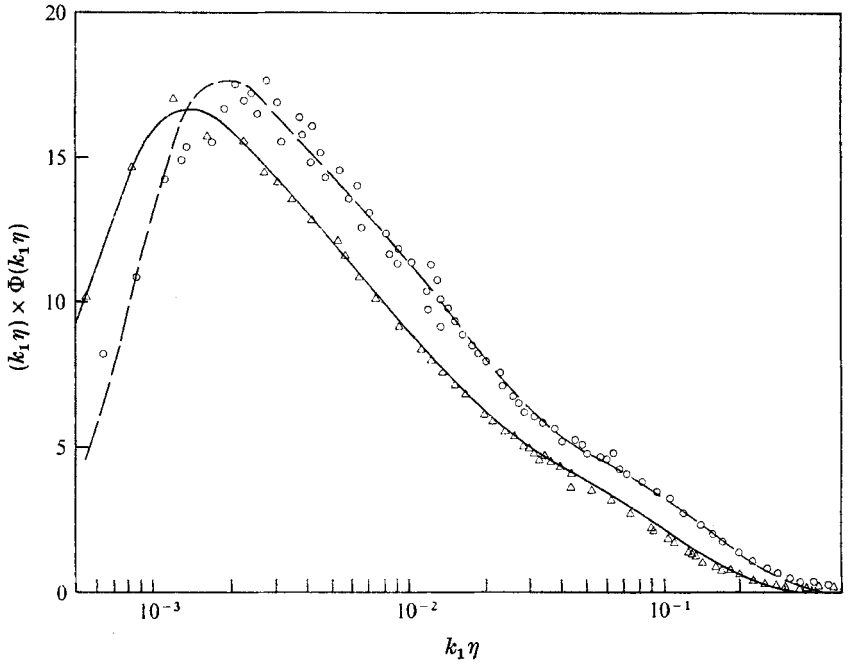

FIGURE 9. Isotropic comparison for present grid data. △, measured u spectrum points; ——, polynomial fit to u spectrum; ○, measured v spectrum points; – – –, isotropic v spectrum predicted from u polynomial fit.

Measurements yielding $u' \neq v'$ have little relevance to the question of isotropy of small-scale motions in the flow. This is an important point, since the theories of universal similarity depend on the isotropy of the small-scale turbulent motions.

As a test of local isotropy at small scales, we have chosen to compare the longitudinal and transverse spectra according to the isotropic relationship:

$$\Phi_2^*(k_1\eta) = \tfrac{1}{2}[\Phi_1(k_1\eta) - (k_1\eta)\,\partial\Phi_1(k_1\eta)/\partial(k_1\eta)]. \tag{23}$$

For these comparisons the normalized spectra including wire-length corrections were used. A polynomial fit was made to the measured longitudinal (Φ_1) spectral data points, as shown in figure 9. The maximum deviation of the polynomial fit from the Φ_1 spectrum was less than 2 %. Using (23), an isotropically predicted transverse (Φ_2^*) spectrum was computed from the polynomial fit to Φ_1. The measured transverse spectrum is compared with the predicted isotropic transverse spectrum in figure 9. The first moments of the velocity spectra are plotted versus normalized wavenumber in semi-log co-ordinates in order to show the comparison more clearly. The measured and isotropically predicted transverse spectra are in excellent agreement up to a normalized wavenumber of 0·1, with an average deviation of less than 5 %. In this region the empirical wire-length corrections are less than 15 % of the measured value. Only at the largest scales (smallest wavenumber) does the deviation from the isotropic relation reach 10 %. Figure10 presents similar results for the data of Kistler & Vrebalovich (1966) at their highest Reynolds number ($R_M = 2{\cdot}4 \times 10^6$), where $u'/v' = 1{\cdot}23$. The data only appear isotropic at the very high wavenumbers. This plot clearly shows that

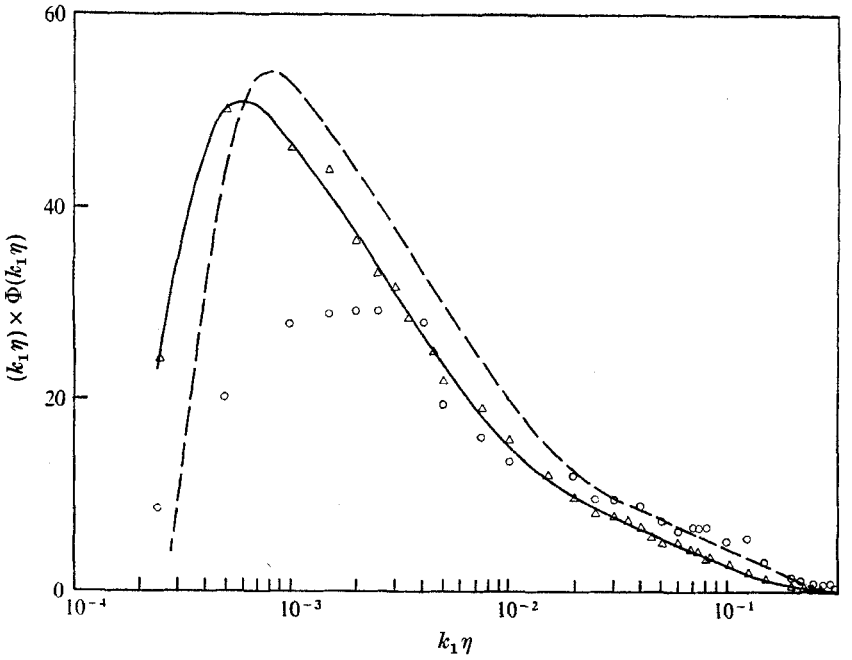

FIGURE 10. Isotropic comparison for data of Kistler & Vrebalovich for $R_M = 243 \times 10^4$ and $R_\lambda = 670$. △, measured u spectrum points; ——, polynomial fit to u spectrum; ○, measured v spectrum points; – – –, isotropic v spectrum predicted from u polynomial fit.

the anisotropy indicated by u'/v' is due to the large energy-containing scales. The deviation from isotropy begins below $k_1\eta = 0{\cdot}02$, which from figure 8 is in the centre of their inertial subrange.

As a final check on isotropy we can examine the derivative measurements. In contrast to the u' and v' measurements, the values of the mean-square velocity derivatives are very sensitive to the small-scale turbulent fluctuations. Unfortunately, this is the region where effects of finite wire length become most important. For isotropic turbulence one should find $\overline{(\partial u/\partial x_1)^2} = 0{\cdot}5\overline{(\partial v/\partial x_1)^2}$. The actual ratio of the measured values in table 1 is 0·59 rather than 0·5. Inasmuch as we have previously demonstrated isotropy at larger scales, it seems highly unlikely that the discrepancy can be interpreted as anisotropy of the small scales. The difference is probably due to differences in the wire-length attenuation of the longitudinal and transverse spectra. Wyngaard's theoretical wire-length correction as well as the empirical correction indicate a larger attenuation for the transverse spectrum than for the longitudinal spectrum. By integrating the empirically corrected dissipation spectra Ψ_1 and Ψ_2 the relation is found to be $\overline{(\partial u/\partial x_1)^2} = 0{\cdot}42\overline{(\partial v/\partial x_1)^2}$. The ratio is considerably changed, though still not equal to 0·5. However, the value lies within the uncertainty of the empirical wire-length corrections.

4. Summary

High Reynolds number measurements were made in a grid-generated turbulent flow in order to determine the inertial subrange constant α_1 at a Reynolds number between the low values usually obtained in laboratory flows and the large values obtained in geophysical flows. When this experiment was begun, reported values of α_1 in geophysical flows ranged from 0·4–0·7, while the only available high Reynolds number laboratory study yielded an α_1 value of 0·7–0·9. Subsequently, a number of determinations of α_1 in geophysical flows have been reported. Nasmyth (1970) re-examined the data of Grant, Stewart & Moilliet (1962), and made corrections leading to a value of 0·56. Paquin & Pond (1971) obtained a value of $\alpha_1 = 0{\cdot}55$, while McBean *et al.* (1971) suggested a value of 0·60 as most appropriate.

The value of α_1 obtained in our present experiment was $0{\cdot}48 \pm 0{\cdot}06$. This value seems to be in agreement with recent determinations. Our results indicate that α_1 values for large Reynolds number laboratory grid turbulence are not significantly different or larger than those obtained in high Reynolds number atmospheric or oceanic turbulent flows.

For the measurements reported in this paper the spectra exhibit good agreement with isotropic predictions over the range of wavenumbers that can be reasonably assumed to be only slightly affected by wire-length averaging. This result is in contrast to that of Kistler & Vrebalovich, whose data show considerable anisotropy in the energy-containing scales. Our closer approach to isotropy, moreover, seems to be more in agreement with the general trend toward greater isotropy with increasing Reynolds number that is seen in the data of Comte-Bellot & Corrsin (1966).

In order to reconcile our direct dissipation measurements with decay law values a new wire-length correction procedure was devised. Comparison was made with a reference spectrum assuming universal similarity. The results of our empirical wire-length correction indicate that Wyngaard's (1968) theoretical correction, based on Pao's (1965) spectrum, is not adequate for our particular wire length and separation. The actual corrections for the spectra are seriously underestimated by the theoretical corrections. It is suggested that a systematic experiment should be performed to determine the range of reliability of the theoretical wire-length correction.

One author (GRS) would like to acknowledge the valuable assistance of G. Murphy and J. A. Garrison in setting up the experiment, and of S. K. Najak and W. Edling in performing the experiment. The authors are particularly grateful to F. H. Champagne and C. H. Friehe for their many helpful suggestions. Financial support at Colorado State University was provided by Project THEMIS, sponsored by the Office of Naval Research under Contract N0014-68-A-0493-0001, Project NR062-414/6-6-68 (Code 438). Analysis of the data was supported at Princeton University by NONR Contract N00014-67-A-0151-0031, Project NR083-279. Financial support at the University of California-San Diego was provided primarily by NONR Contract N00014-69-A-0200-6006 and

partially by ARPA Contract DA-31-124-ARO-D-257 and NSF Grant GA-28366. J. Schedvin was the recipient of an NSF Fellowship during the course of this work.

REFERENCES

BRADSHAW, P. 1967 *Nat. Phys. Lab. Aero. Rep.* no. 1220.

CERMAK, J. E. 1971 *A.I.A.A. J.* **9**, 1746.

CHAMPAGNE, F. H. 1973 *Bull. Am. Phys. Soc.* II, **18**, 1468.

COMTE-BELLOT, G. & CORRSIN, S. 1966 *J. Fluid Mech.* **25**, 657.

COMTE-BELLOT, G. & CORRSIN, S. 1971 *J. Fluid Mech.* **48**, 273.

CORRSIN, S. 1958 *N.A.C.A. Rep.* RM58B11.

FRIEHE, C. A. & SCHWARZ, W. H. 1970 *J. Fluid Mech.* **44**, 173.

GIBSON, C. H., STEGEN, G. R. & MCCONNELL, S. 1970 *Phys. Fluids*, **13**, 2448.

GIBSON, C. H., STEGEN, G. R. & WILLIAMS, R. B. 1970 *J. Fluid Mech.* **41**, 153.

GRANT, H. L., STEWART, R. W. & MOILLIET, A. 1962 *J. Fluid Mech.* **12**, 241.

KISTLER, A. L. & VREBALOVICH, J. 1966 *J. Fluid Mech.* **26**, 37.

KOLMOGOROV, A. N. 1962 *J. Fluid Mech.* **13**, 82.

LUMLEY, J. L. 1965 *Phys. Fluids*, **8**, 1056.

MCBEAN, G. A., STEWART, R. W. & MIYAKE, M. 1971 *J. Geophys. Res.* **76**, 6540.

NASMYTH, P. W. 1970 Dissertation, University of British Columbia.

PAO, Y. H. 1965 *Phys. Fluids*, **8**, 1063.

PAQUIN, J. E. & POND, S. 1971 *J. Fluid Mech.* **50**, 257.

POND, S., PHELPS, G. T., PAQUIN, J. E., MCBEAN, G. & STEWART, R. W. 1971 *J. Atmos. Sci.* **28**, 901.

POND, S., SMITH, S. D., HAMBLIN, P. F. & BURLING, R. W. 1966 *J. Atmos. Sci.* **23**, 376.

POND, S., STEWART, R. W. & BURLING, R. W. 1963 *J. Atmos. Sci.* **20**, 319.

STEWART, R. W. & TOWNSEND, A. A. 1951 *Phil. Trans.* A **243**, 359.

WYNGAARD, J. 1968 *J. Sci. Instrum.* **1**(2), 1105.